Hindawi
Advances in Materials Science and Engineering
Volume 2023, Article ID 9508173, 17 pages
https://doi.org/10.1155/2023/9508173

Research Article

Mechanical Properties of Deep Variable Dip Joint Rock Mass in Reservoir Area under Wet and Dry Conditions

Fei Li,[1,2,3] **Huafeng Deng**,[1,3] **Wenwen Liu**,[4] **and Guoyong Duan**[1,5,6]

[1]*Key Laboratory of Geological Hazards on Three Gorges Reservoir Area (China Three Gorges University), Ministry of Education, Yichang, Hubei, China*
[2]*College of Civil Engineering, Hubei Three Gorges Polytechnic, Yichang, Hubei, China*
[3]*College of Civil Engineering and Architecture, China Three Gorges University, Yichang, Hubei, China*
[4]*Hubei Xinmin Construction Group Co. LTD, Yichang, Hubei, China*
[5]*Hubei Provincial Engineering Technology Research Center for Power Transmission Line, China Three Gorges University, Yichang, Hubei, China*
[6]*College of Electrical Engineering and New Energy, China Three Gorges University, Yichang, Hubei, China*

Correspondence should be addressed to Guoyong Duan; duanguoyong@ctgu.edu.cn

Received 4 July 2022; Accepted 10 August 2022; Published 29 April 2023

Academic Editor: Depeng Ma

The mechanical property of deep complex jointed rock mass is a hot topic in rock mechanics. In order to grasp the deformation and damage rules of through-going variable dip joint rock masses, the triaxial compression test and joint surface morphology scan test were conducted on cylindrical specimens in dry and wet conditions under 0, 5, 10, and 20 MPa water pressure. Through these tests, the deterioration law of rock samples under different pore water pressure in dry and wet conditions was studied. The effect of pore water pressure on the strength of saturated jointed rock sample is nonlinear. The imposed pore water pressure can significantly increase the axial deformation of rock samples, and higher pore water pressure can facilitate the deformation deterioration of samples. When the pore pressure is high, the rock samples show the characteristics of sliding shear failure. Under different pore pressure, the compressive strength of dry jointed rock is significantly higher than that of saturated jointed rock, and the saturated rock is more susceptible to sliding in the joint plane than dry rock. Dry jointed rock samples have stronger deformation ability than saturated jointed rock samples. The change rate of the morphologic parameters and the distribution of the failure cracks indicate that the stress concentration is evident in the middle of the joint plane.

1. Introduction

Reservoir earthquakes are one of the problems encountered during water resource development and utilization. Tens of thousands of earthquakes, large and small, have occurred since the Three Gorges Reservoir was impounded, and nearly one-third of them [1, 2] are inextricably linked to the local Gaoqiao Fault (Figure 1) [3–6]. Under the effect of vertical load loading and unloading brought by the periodic change of reservoir water, which triggers the increase of elastic stress of the reservoir base rock, the rise in pore water pressure is caused by the compaction of the rock pore, the change of groundwater level, and the diffusion of reservoir water outside the reservoir area, and the deterioration of mechanical rock properties leads to fault rupture and induces reservoir earthquake.

Many scholars have studied the mechanical properties of jointed rock mass, focusing on single jointed rock samples. Nonhole connected jointed rock masses with different connectivity rates exhibit anisotropic mechanical properties under loading and unloading conditions [7], and the joint direction has a greater effect on the strength and deformation of the rock mass than joint connectivity [8]. Renani established linear and nonlinear failure criteria using an analytical model of rock masses with nonpenetrating joints and predicted that increasing the joint strength and

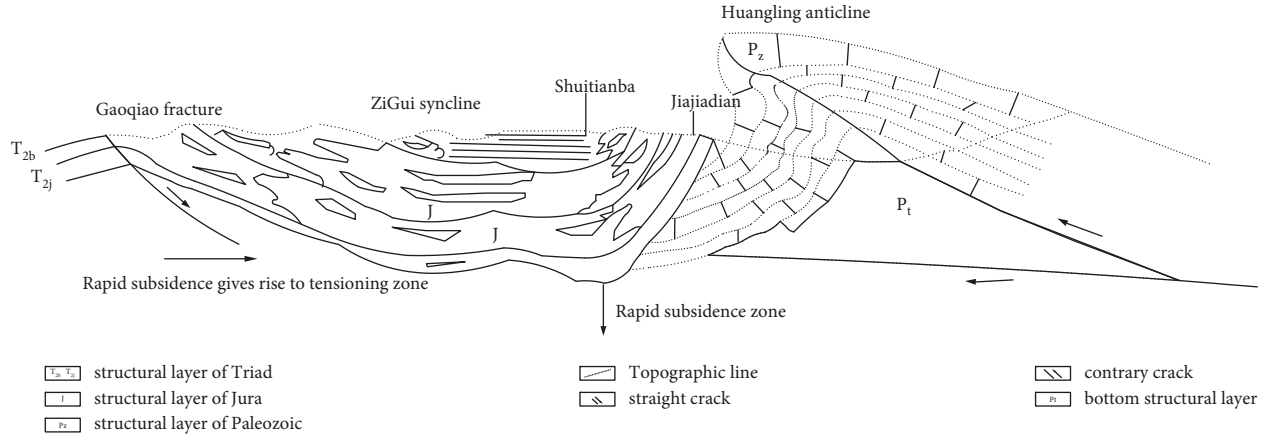

Figure 1: Profile of Gaoqiao fracture formation mechanism.

decreasing the joint shear strength would reduce the bond and friction of rock mass strength [9]. In terms of the failure mechanism of the jointed rock mass, Liu investigated the fatigue mechanism of the jointed rock mass under cyclic loading conditions from an energy perspective through routine tests [10]. The ductility of the joint with the magnitude of the positive stress has a significant influence on the fracture roughness and residual shear modulus of the rock bridge, which can be of great help in assessing the resistance of the rock bridge to evaluate the stability of the rock excavation [11]. However, there are fewer studies on rock masses with variable dip joints.

In terms of dry and wet states, current studies have demonstrated that the mechanical properties of rock samples in water-saturated states deteriorate significantly [12]. The deterioration of rock samples is exacerbated by the water-mechanical-chemical coupling state of mechanical loading and chemical interaction [13, 14]. Acoustic emission signals indicated that various shear-tensile damage modes or rock bridge modes occur in dry and saturated samples during rock failures [15], and rock moisture properties affect the peak strength, plastic deformation, and strength of rock failure [16].

Nicolas et al. [17] suggest that water mainly affects the diffusion aspect of rock samples in the brittle phase and has a more negligible effect on the peak strength. Tang [18] found that the peak shear strength decreases in dry and saturated fractures, where the shear parameter has a negative exponential trend, but the mechanical properties evolve differently. The diffusion of pore water pressure causes the activation of rock faults and the release of elastic energy [19], mainly manifest as the decrease of strength and the deterioration of deformation properties of rock masses. Li [20, 21] found that the permeability of dolomite is positively correlated with pore water pressure by the NMR technique, and the strength and the deformation properties of sandy slate decreased with increasing water pressure. Water pressure affects cohesion, deformation modulus, and internal friction angle differently. The cohesive force decreases sharply with the increased water pressure until the coherent power is lost. In rock mechanics indoor tests, most studies generalize natural joints as linear or planar, and the fugacity form is either through joints or nonthrough joints [11, 22, 23], which cannot realistically describe the actual joints morphology and in fact, different strata and fractures are primarily curved. This study simulates the rapid change of pore water pressure in the rock layer triggered by the short-time rise and fall of the water level in the reservoir area under different dry and wet conditions of the original stratum. Successive variable dip joints were set in the tuff rock samples to simulate the real fracture orientation to investigate the deterioration of mechanical properties under pore water pressure. The results can help understand the mechanical properties and damage modes of faults when rupture occurs, providing some reference to analyze the cause of earthquakes in the Three Gorges reservoir area.

2. Materials and Tests

2.1. Material and Rock Specimen Preparation. In this test, the tuffs of the Triassic Badong Formation near the Gaoqiao Fault in the Three Gorges Reservoir area were first drilled and core sampled into cylindrical rock samples with a diameter of 50 mm and a height of 100 mm (Figure 2(a)). The waterjet was used to cut out a joint surface with a gradual change in dip angle from 40° to 20° in the sample, which was used to simulate the production of the Gaoqiao fracture. A hole was punched in the center of the lower half of the rock sample to facilitate the application of water pressure (Figure 2(b)).

In this study, rock samples in both dry and saturated states were used, and a total of 8 working conditions with 4 levels of water pressure were applied, 2–3 rock samples for each condition. The saturation method was performed by vacuum saturation.

2.2. Test Procedure

2.2.1. Rock Mechanics Test Procedure. The rock samples were loaded with axial pressure (rate: 2 MPa/min) and circumferential pressure (rate: 1 MPa/min) simultaneously, reaching 100 MPa (axial pressure) and 50 MPa

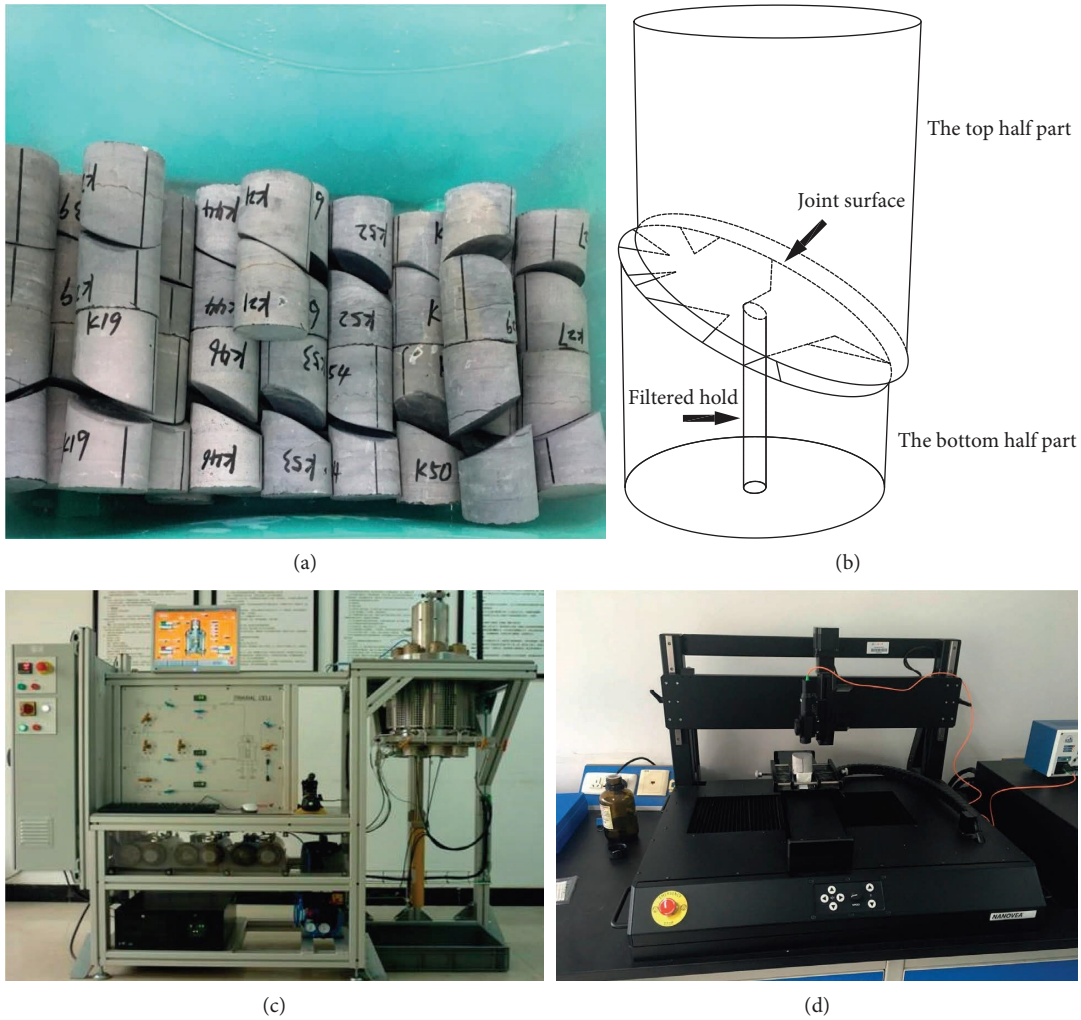

Figure 2: (a, b) Limestone rock specimens and (c, d) test equipment.

(circumferential pressure), respectively; keeping the circumferential pressure axial pressure unchanged, the water pressure was loaded to 0 MPa, 5 MPa, 10 MPa, and 20 MPa (2–3 rock samples were used for each level of water pressure test), and the water pressure loading rate was 1 MPa/min. After the water pressure was loaded to a predetermined value, anisotropic stress of rock samples was maintained for 30 minutes, and then the axial pressure continued to increase (at a rate of 2 MPa/min) until the failure occurred.

2.2.2. Analysis of the Fine Morphological Characteristics of the Joint Surface. A three-dimensional morphological scanner was used to scan the microscopic morphological characteristics of the joint surface of the rock sample before and after the test.

2.3. Test Equipment. The main equipment are TOP INDUSTRIE rock triaxial tester (Figure 2(c)), ST500 3D noncontact surface profiler (Figure 2(d)), and so on.

2.4. Stress-Strain Relation. The stress-strain curves of jointed rock specimen during the test are shown in Figure 3.

3. Mechanical Test Results of Variable Dip Nodular Rock Samples under Different Water Pressure

3.1. Stress-Strain Curve. The stress-strain curves of the jointed rock samples during the test are shown in Figure 3.

The pore water pressure was applied to the dry jointed rock sample, and the water pressure acted directly on the joint surface through the small holes in the lower part of the rock sample. From Figures 3(a)–3(d), it can be seen that with the increase of pore water pressure, the transverse strain of the rock sample has a tendency to gradually decrease, and the proportion of the plastic deformation stage in the test process further decreases. It should be noted that the transverse strains of the dry samples all tend to decrease in the front part when the pore water pressure is 5 MPa but start to increase gradually near the time of damage, which is caused by the rupture of the sheath that wraps the rock samples.

The triaxial compression tests were carried out on saturated jointed rock samples with different pore water pressures, and the stress-strain curves are shown in

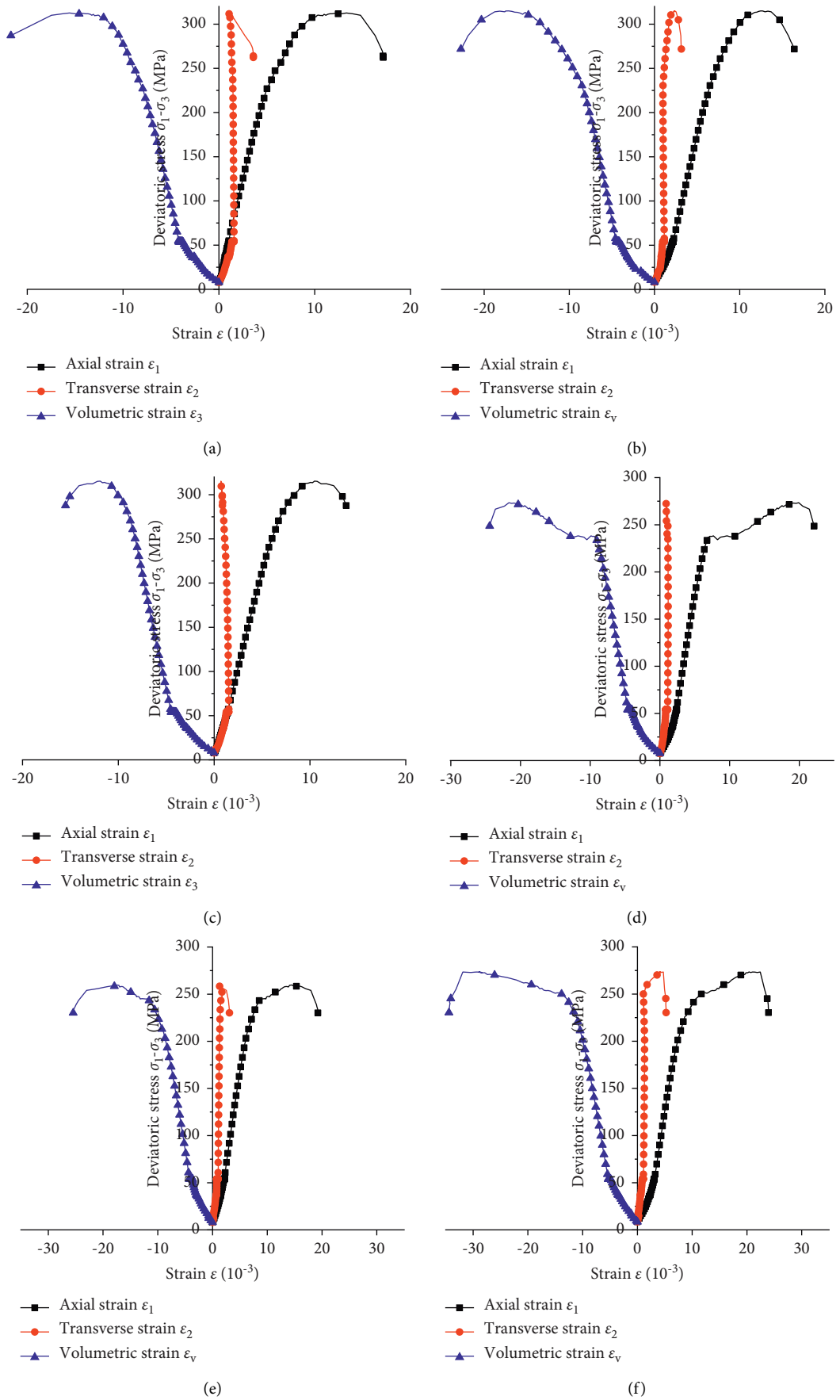

Figure 3: Continued.

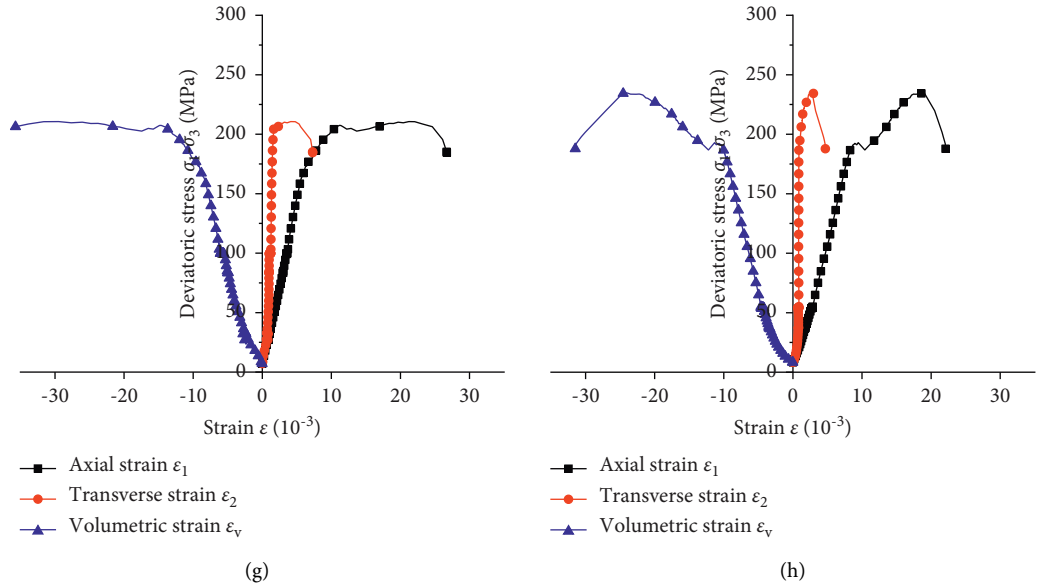

Figure 3: Stress-strain curves of jointed rock specimens under different pore pressures in wet and dry conditions.

Figures 3(e)–3(h). The saturated rock samples showed obvious plastic deformation during the test, and the proportion of plastic deformation before damage tended to rise with the increase of pore water pressure. During the loading process, the rate of change of transverse strain is much smaller than that of axial strain, but it suddenly rises when the rock sample approaches the peak strength of the first section until the rock sample is destroyed. For the axial strain, strain hardening occurs to varying degrees as the rock sample approaches the peak strength, i.e., the material must increase the stress to continue the strain after yield slip, and the ability of the material to resist deformation is improved at this stage. Observing the stress-strain curves, it can be seen that the rock samples under water pressure of 20 MPa have more sampling points in the strain-hardening stage than other water pressure conditions, while the strain in the elastic stage is smaller, indicating that the rock samples under higher water pressure enter the strain-hardening stage earlier while becoming less brittle.

The strain-hardening phenomenon of the saturated samples was most obvious at the pore water pressure of 20 MPa, the rock samples reached the first peak strength at the end of the elastic stage, and the second peak strength appeared after further loading was significantly higher than the first peak strength. However, the total peak strength is significantly smaller than that of the rock samples under pore water pressure of 0, 5, and 10 MPa.

3.2. Strength Characteristics. When the surrounding pressure is constant, the peak strength of the dry nodular rock samples shows a decreasing trend at different pore water pressures (Figure 4(a)).

Through data fitting, the relationship between water pressure of saturated sample and triaxial compressive strength can be obtained:

$$\sigma_1 = \frac{P_0}{18.758 - 0.965P_0} + 339.400. \quad (1)$$

The correlation coefficient R^2 was 0.9992. According to Figure 4(a) and the fitting (1), it can be seen that at low pore water pressure (0, 5, and 10 MPa), the triaxial compressive strength of dry jointed rock samples did not show large changes; when the pore water pressure increased to 20 MPa, the triaxial compressive strength showed a significant decrease; the minimum value of rock sample strength decreased about 11% compared with the maximum value.

The pore water pressure reaches the threshold value of 10 MPa before the strength of the rock sample is greatly deteriorated and has a significant impact on the rock properties. Considering that there are a large number of micropores in the rock sample, the lower pore water pressure is not enough to make the pores inside the rock sample rupture and connect, and the pores still have the pressure-bearing capacity at this time; when the pore water pressure increases, the micropores gradually connect with each other and produce obvious damage to the rock sample, which leads to the strength decrease.

Under the influence of different pore water pressure, the triaxial compressive strength of saturated nodular rock samples shows a phase change (Figure 4(c)).

Through data fitting, the relationship between water pressure of saturated sample and triaxial compressive strength can be obtained:

$$\sigma_1 = \frac{P_0}{0.897 - 0.128P_0} + 284.517. \quad (2)$$

The correlation coefficient R^2 was 0.97025. According to Figure 4(c) and the fitting (2), the maximum value of triaxial compressive strength occurs at 5 MPa pore water pressure and the minimum value occurs at 10 MPa pore

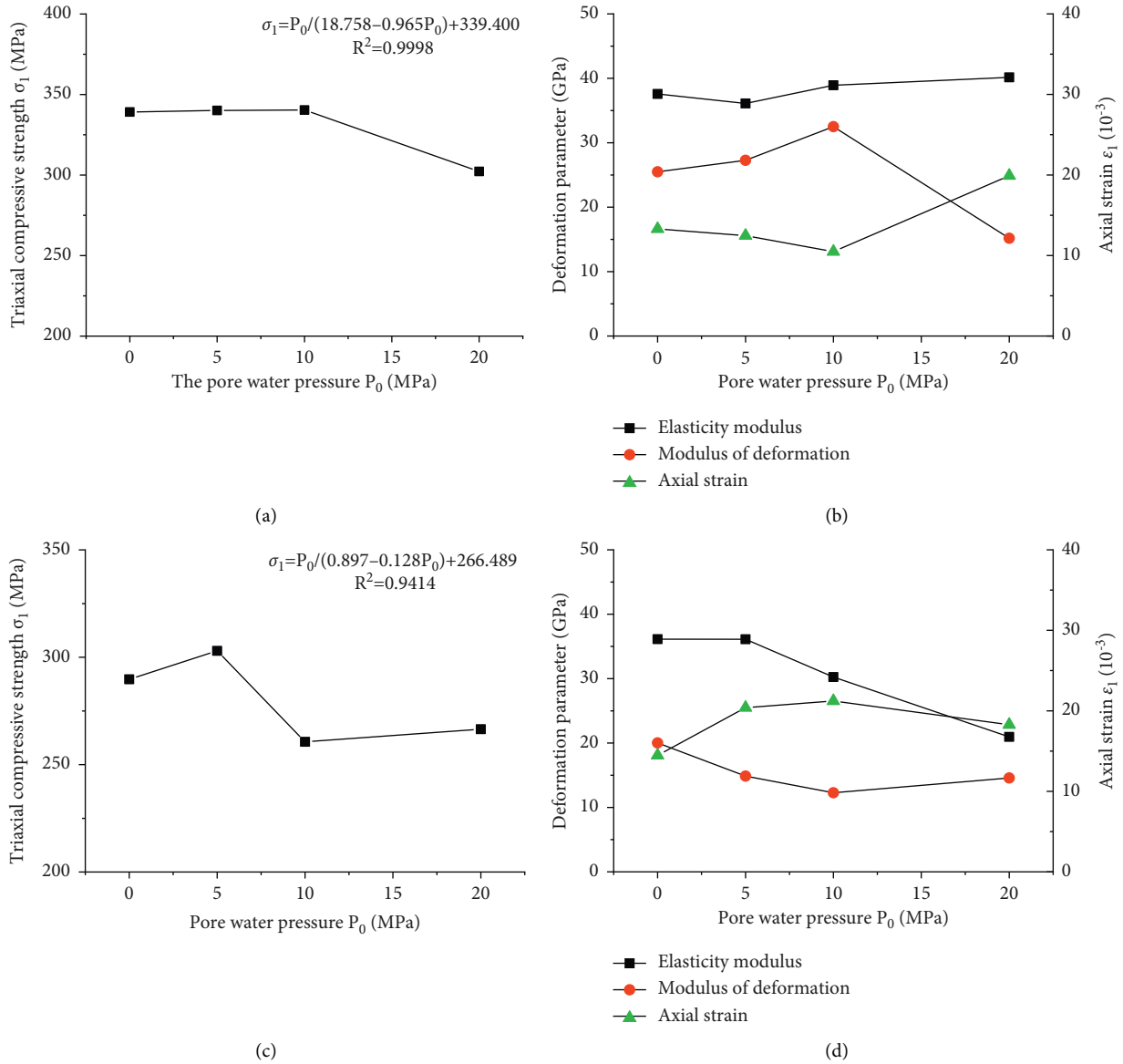

Figure 4: Strength and deformation curves of rock specimens in different states in wet and dry conditions.

water pressure. The triaxial compressive strength of the rock samples is closer at 0 and 5 MPa of pore water pressure; the triaxial compressive strength of the rock samples is closer at 10 and 20 MPa of pore water pressure. Therefore, it can be divided into two stages: the first stage with pore water pressure of 0–10 MPa and the second stage with pore water pressure of 10–20 MPa, and the compressive strength of the second stage decreased by about 13%. The pore water pressure is 5 MPa, and the measured value at this time has a large deviation from the fitted value, which is mainly due to the discrete nature of the specimen. For saturated nodular rock samples, the phase change of strength indicates that the effect of pore water pressure on strength is nonlinear, and the strength of rock samples changes significantly only when the pore water pressure changes by an order of magnitude.

3.3. Rock Deformation Characteristics. The elastic modulus and deformation modulus of dry nodular rock samples under different pore water pressure are shown in Figure 4(b), the difference between elastic modulus and deformation modulus is closer when the pore water pressure is 0, 5, and 10 MPa, indicating that the deformation of rock samples before reaching the peak strength under the application of lower pore water pressure is dominated by elastic deformation, and the proportion of plastic deformation is very small. In the process of increasing the pore water pressure from 0 MPa to 10 MPa, the deformation parameter values showed an increasing trend, while the peak strength did not change significantly, and the axial deformation of the specimen when the damage occurred under the lower pore water pressure showed a decrease. When the pore water pressure

increased to 20 MPa, the axial deformation showed a large increase. At lower pore water pressure, the stress concentration of internal microfractures is partially eliminated due to the adsorption of dissolved pores or microporosity near the surface of the rock sample, which makes the axial deformation rate of the specimen decrease. When the pore water pressure increased to 20 MPa, a larger deformation appeared in the axial direction, at which time the pore water pressure promoted the mutual penetration between micropores, which showed that the time from the initial loading to the final damage was shortened, indicating that the higher pore water pressure had an obvious effect on the deterioration of the specimen.

The deformation parameters of the saturated nodular rock samples under different pore water pressures are shown in Figure 4(d). The maximum value of the elastic modulus appears at the pore water pressure of 0 MPa and the minimum value appears at the pore water pressure of 20 MPa; the maximum value of the deformation modulus also appears at the pore water pressure of 0 MPa, but the minimum value appears at the pore water pressure of 10 MPa. According to the trend of deformation parameters with pore water pressure, the elastic modulus and deformation modulus both show a decreasing trend with the increase of pore water pressure, and the variation between the maximum and minimum values is about 25%. The axial strain of the rock samples showed an overall increasing trend with the increase of pore water pressure, and the maximum value of axial strain increased by about 50%, compared with the minimum value. It can be concluded that the application of pore water pressure can significantly increase the axial deformation of the rock samples but weaken the elastic deformation and enhance the plastic deformation capacity of the rock samples.

3.4. Damage Characteristics. The coarse solid line is the primary crack, and the fine solid line is the secondary crack.

As shown in Figures 5(a)–5(d), the common characteristics of the damage of dry nodular rock samples under different pore water pressure are obvious primary cracks and more secondary cracks concentrated in the lower part, and this phenomenon indicates that the softening effect of the rock samples is more obvious the closer to the pore water pressure source during the loading damage. Under the action of different pore water pressure, the damage characteristics show different characteristics. From the damage characteristics of rock samples before and after the application of pore water pressure (Figures 5(a) and 5(b)), it can be found that the cracks in the lower part of the rock samples increase significantly after the application of pore water pressure, and the distribution also shows a certain pattern with the change of pore water pressure. When the pore water pressure is 5 MPa, the primary and secondary cracks are partially parallel to the rock sample axis at the initial stage and then deflected, showing signs of cleavage and shear damage. When the pore water pressure rises to 10 MPa and 20 MPa, the main feature of crack orientation is a deviation from the axis at a certain angle, showing the characteristics of shear damage. At the pore water pressure of 20 MPa, a large number of secondary cracks were produced in the lower part of the rock sample.

The damage characteristics of the saturated sample under different pore water pressure are shown in Figures 5(e)–5(h). When the pore water pressure is 0 MPa, i.e., no pore water pressure is applied, the cracking trend of the rock sample is from horizontal and inclined to flat main cracks through the lower part of the rock sample, accompanied by secondary cracks. When the pore water pressure is 5 MPa, the main crack penetrates the whole rock sample through the middle of the joint surface, and the rock sample shows obvious shear damage characteristics. When the pore water pressure is 10 MPa, the main crack appears in the lower part of the sample, and the horizontal and inclined cracks extend to the bottom edge of the sample, mainly caused by the sliding and pulling of the upper and lower parts along the joint surface. When the pore water pressure is 20 MPa, the main crack penetrates through the center of the joint surface in the upper and lower parts of the sample, there are more cracks in the upper part than in the lower part, and secondary cracks are produced between the parallel main cracks.

The above phenomenon indicates that the elevated pore water pressure greatly weakens the shear strength of the rock sample. Since the joint surface has a certain roughness, during the sliding process of the rock sample along the joint surface, multiple stress concentrations occur on the joint surface and cause the generation and expansion of cracks. At the same time, different pore water pressures lead to different damage patterns of the jointed rock mass.

4. Analysis of the Effect of Pore Water Pressure on the Degradation of Variable Dip Nodular Rock Samples

4.1. Effect of Pore Water Pressure on Strength Properties of Saturated and Dry Nodular Rock Samples. For the nodular rock samples, the different states (dry or saturated) had significant effects on the strength of the rock samples, as shown in Figure 6. Under the influence of different pore water pressures, the compressive strength of the nodular dry rock samples was higher than that of the nodular saturated rock samples with the same water pressure. The compressive strengths of dry rock samples were 17.0%, 12.2%, 30.6%, and 13.4% higher than those of saturated rock samples under the pore water pressure of 0 MPa, 5 MPa, 10 MPa, and 20 MPa, respectively. During the loading damage, the friction coefficient of the joint surface of the dry rock samples was larger, and the friction coefficient of the joint surface of the saturated rock samples was smaller due to the influence of pore water. Therefore, the dry joint surface can provide a larger friction force during the loading damage, which makes the rock samples have a higher bearing capacity. The saturated rock samples are more prone to slip of the joint surface than the dry rock samples, so the load-bearing capacity of the saturated rock samples is lower.

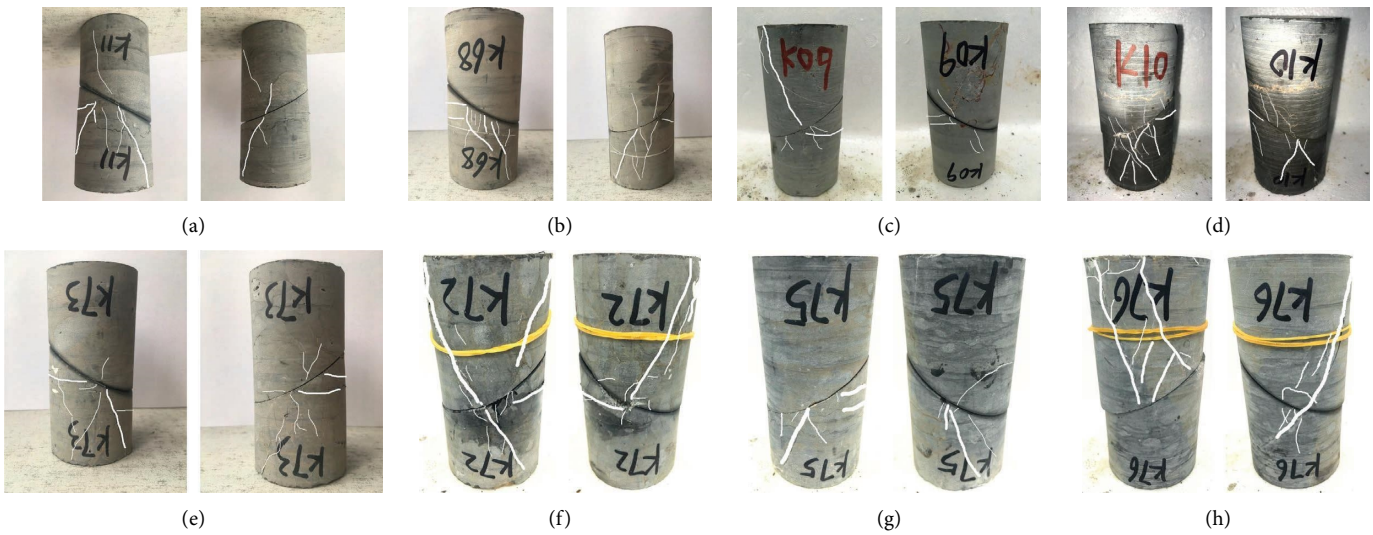

Figure 5: Failure characteristics of jointed rock specimens under different pore pressure in wet and dry conditions (The coarse solid line is the primary crack, and the fine solid line is the secondary crack).

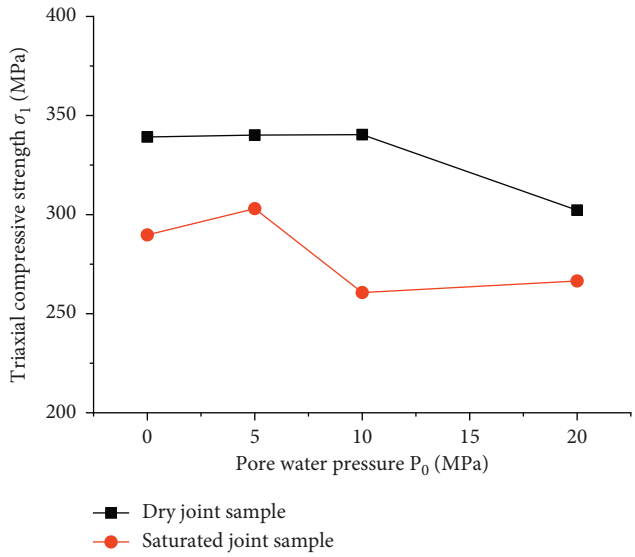

Figure 6: Strength comparison of rock specimens in different states.

4.2. Influence of Pore Water Pressure on Deformation Parameters of Saturated and Dry Nodular Rock Samples. Dry nodular rock samples at lower pore water pressure partially eliminate the stress concentration of internal microfractures due to the adsorption of the dissolved pores or microporosity near the surface of the rock samples, which decreases the axial deformation rate of the specimens. When the pore water pressure continues to increase, the micropores penetrate each other, which shows that the time from the initial loading to the final damage is shortened and the deformation appears to be larger growth, indicating that the effect of higher pore water pressure on the deterioration effect of the specimen is more obvious.

The elastic modulus and deformation modulus of saturated nodular rock samples both show a decreasing trend with the increase of pore water pressure, and the variation between the maximum and minimum values is about 20%–30%. The axial strain of the rock samples showed an overall increasing trend with the increase of pore water pressure, and the maximum value of axial strain increased about 50% compared with the minimum value. It can be concluded that the applied pore water pressure can significantly increase the axial deformation of the rock samples but weaken the elastic deformation and enhance the plastic deformation.

The comparison of deformation parameters of rock samples in dry and saturated states is shown in Figure 7. At 0–5 MPa, the difference between the elastic modulus of rock samples in the dry state and that in the saturated state is small, and at 5–20 MPa, the elastic modulus of rock samples in the saturated state gradually decreases, while that in the dry state slightly increases, resulting in a larger difference between the two.

From Figure 7(a), it can be seen that the elastic modulus of rock samples in different states is similar in dry and saturated states when the pore water pressure is 0–5 MPa. The modulus of elasticity of dry nodular rock samples is greater than that of saturated nodular rock samples only when the pore water pressure is 10–20 MPa. Under different pore water pressure, the elastic modulus of saturated rock samples fluctuates more and the elastic modulus of dry rock samples fluctuates less, which indicates that saturated rock samples are more sensitive to the change of pore water pressure. By the water pressure setting in accordance with the isometric series, the effect on the strength and deformation of the rock sample is more obvious under the larger water pressure. After exceeding 5 MPa, the larger the water pressure is, the larger the difference of elastic modulus between different states.

The deformation modulus of dry rock samples was 27.3%, 83.6%, 164.5%, and 4.1% higher than that of saturated rock samples at a pore water pressure of 0 MPa, 5 MPa, 10 MPa, and 20 MPa, respectively. In the interval from 0 to 10 MPa, the difference between the deformation modulus of the dry sample and the saturated sample gradually increased.

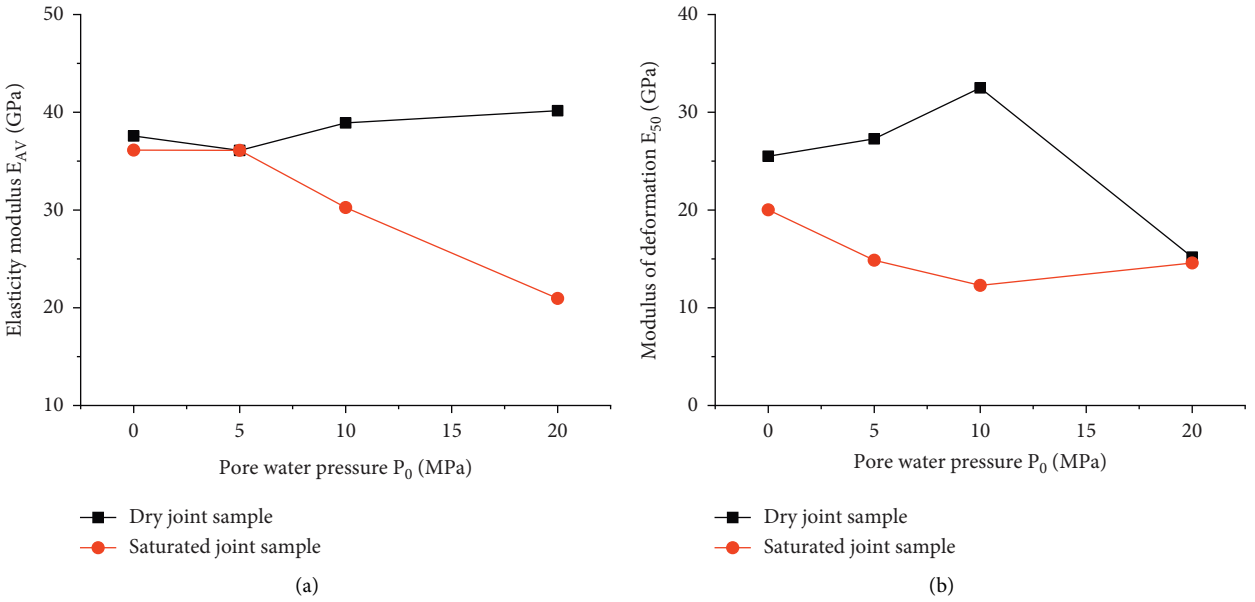

Figure 7: Deformation parameters include Elastic modulus and Deformation modulus.

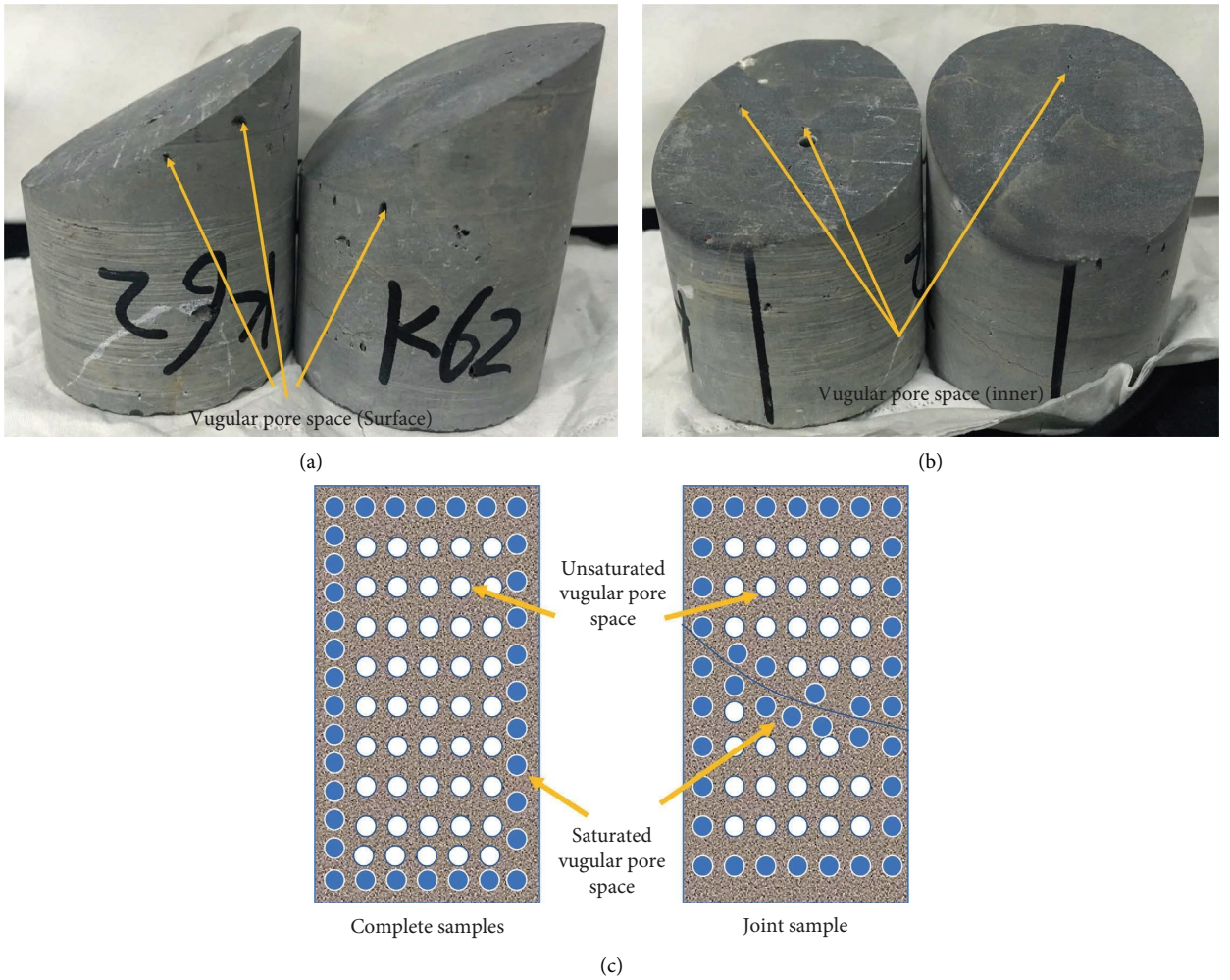

Figure 8: Solution pores in limestone samples (a, b) and schematic diagram of solution pore saturation (c).

However, at 20 MPa, the plastic deformation of the dry sample increased substantially compared with that of 0–10 MPa, and the maximum peak stress became smaller, resulting in a significant decrease in the deformation modulus at 20 MPa; the plastic deformation of the saturated sample increased slightly compared with that of 0–10 MPa, but the maximum peak stress increased substantially compared with that of 0–10 MPa, resulting in a small increase in the deformation modulus at 20 MPa. When the water pressure is 20 MPa, the deformation modulus values of dry and saturated rock samples are closer. The anomaly of deformation modulus at 20 MPa pore water pressure may be caused by the ratio of pore water pressure to axial pressure of 100 MPa reaching a certain threshold value, which reduces the friction coefficient of the variable dip joint surface and leads to the reduction of the strength of the joint surface, that is, the softening effect of water. This phenomenon indicates that the dry jointed rock sample has a stronger deformation capacity than the saturated jointed rock sample, although the fluctuation of deformation parameters of the saturated rock sample is smaller due to the softening effect of water, but the bearing capacity of the dry rock sample is significantly larger, which eventually affects the deformation capacity of the rock sample.

4.3. Characterization of Pore Evolution of Chert Specimens. Observations reveal a variable number and uneven distribution of dissolution pores on the surface and inside the tuff, hereafter referred to as dissolution pores (Figure 8). There are veins intruded in the rock layer, along with some laminations.

During the test, the main factors that produce deterioration of mechanical properties of dry nodular rock samples and saturated nodular rock samples are as follows: the saturation state and the size of pore water pressure. Due to the existence of dissolved pores of different sizes in the chert rock samples (Figures 8(a) and 8(b)), the processes of pore generation, saturation by immersion, interconnection, and formation of microcracks are affected by the pore water pressure (Figure 8(c)). First, the presence of pore water pressure decreases the friction coefficient of the joint surface for both dry and saturated joint rock samples. Second, the pore water gradually expands from the outer layer to the inner layer, which makes the dissolution pore linkage and leads to the increase of fracture penetration, thus reducing the mechanical properties of the rock sample. In addition, when the pore water pressure is less than the tensile strength of the rock sample, the change of the dissolved pore size is not enough to make the pore rupture, and it cannot significantly reduce the effective stress in the rock. This results in the deterioration of the mechanical properties of the joint surface of the rock sample.

5. Morphological Parameters of Nodular Rock Samples

The relevant parameters before and after the test were collected by 3D morphological scanning, and some parameters were selected to analyze the roughness of the joint surface. The rate of change of the following morphological parameters was analyzed by combining the 3D scanned images of the convex and concave surfaces of the joints.

The root mean square height and arithmetic mean height were selected for height parameters; the inverse loading area rate was used for functional parameters; the minimum autocorrelation length was used for spatial parameters to characterize the roughness of the joint surface.

The root mean square height S_q represents the root mean square of the height of each point in the region and characterizes the standard deviation of the height, equation (3) is used to characterize the discrete change in height of each point of the joint surface before and after the test, and the rate of change increases the surface joint surface roughness:

$$S_{q1} = \sqrt{\frac{1}{A}\iint_A Z^2(x, y)dxdy}. \tag{3}$$

Here, S_q represents the root mean square height, A represents the scanning area, and Z represents the high function.

S_a represents the average of the absolute value for the height difference of each point relative to the average surface, as shown in equation (4). It represents the alteration in the mean height of each point in the area. A positive change rate indicates an increase in the average height of each point on the joint wall and an increase in the roughness of the joint wall. On the other hand, a negative change rate indicates a decrease in the average height of each point on the joint wall and a decrease in the roughness of the joint wall:

$$S_a = \frac{1}{A}\iint_A |Z(x, y)|dxdy. \tag{4}$$

Here, S_a represents the arithmetic mean height, A represents the scanning area, and Z represents the high function.

S_{mc} represents the height C satisfying the load area ratio p%, which characterizes the overall concave-convex degree of the joint wall before and after the test. When the rate of change is positive, the curvature of the joint surface increases. A positive change rate indicates an increase in the wear degree for concave surfaces, while it indicates a partially disturbed connection surface due to failure for convex surfaces. When the change rate is negative, the curvature of the joint plane decreases. At this point, the edge part of concave surfaces has greater wear than the middle part, while the convex surface has the opposite.

S_{al} indicates the horizon distance, in which the function of autocorrelation decays rapidly toward the specified value s (default: 0.2). It represents the wavelength of the surface. A larger value indicates a larger wavelength on the surface. A positive change rate indicates a large wear degree of the joint surface, while a negative change rate indicates a small wear degree. The morphology parameters rate of change depends on the wear degree of the joint wall and the failure mode of the rock specimen. Different pore pressure may change joint

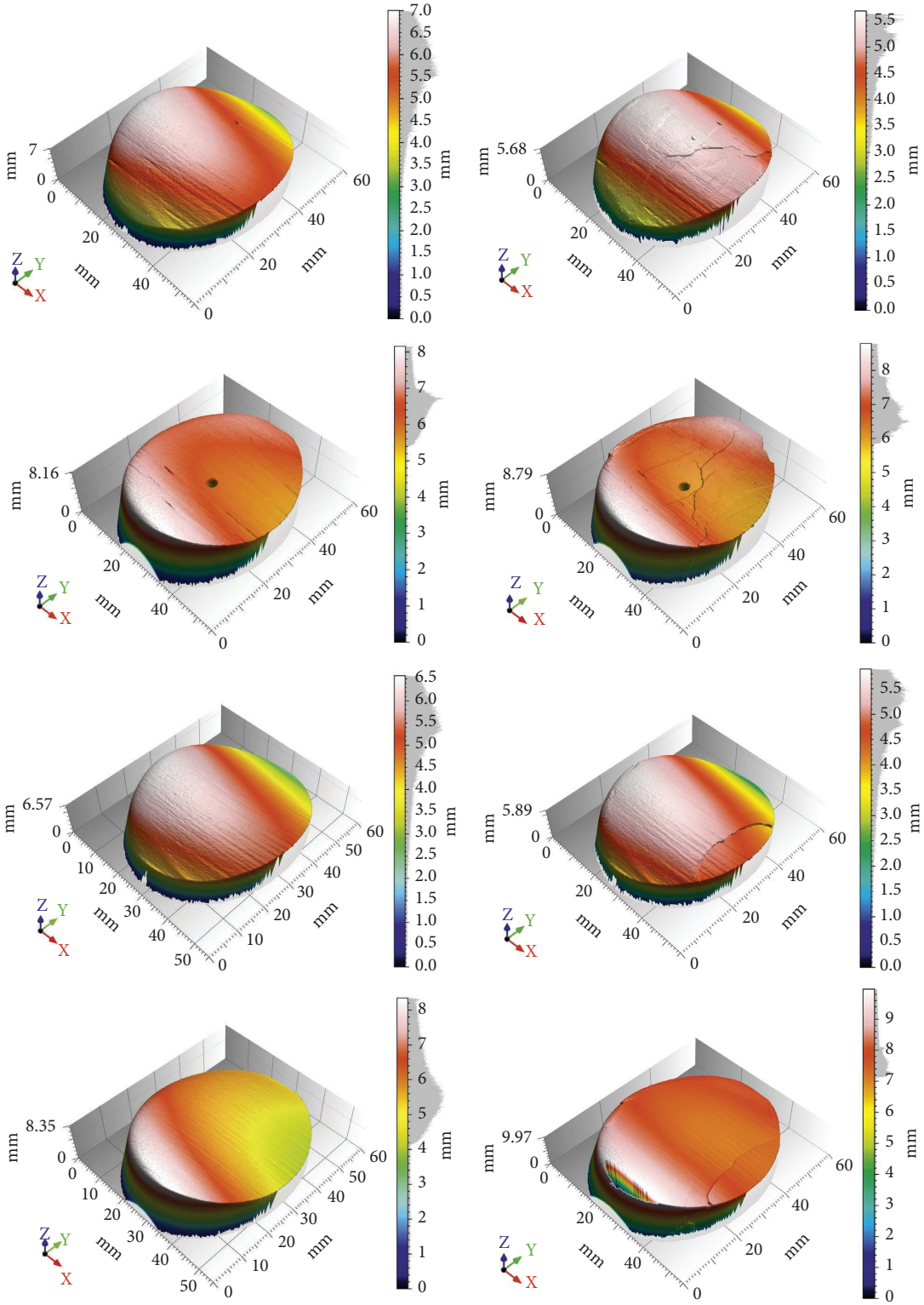

(a)

Figure 9: Continued.

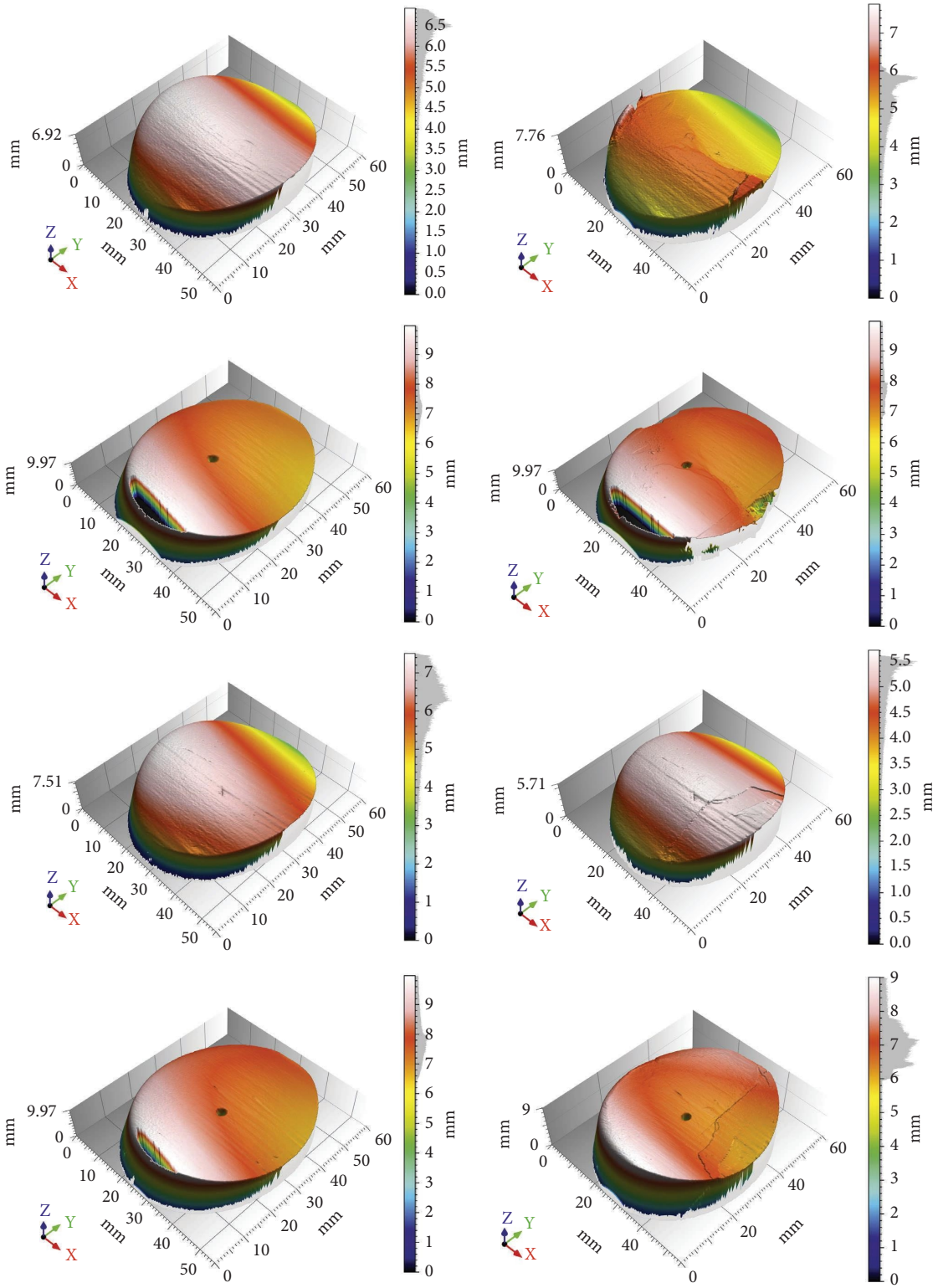

(b)

Figure 9: Continued.

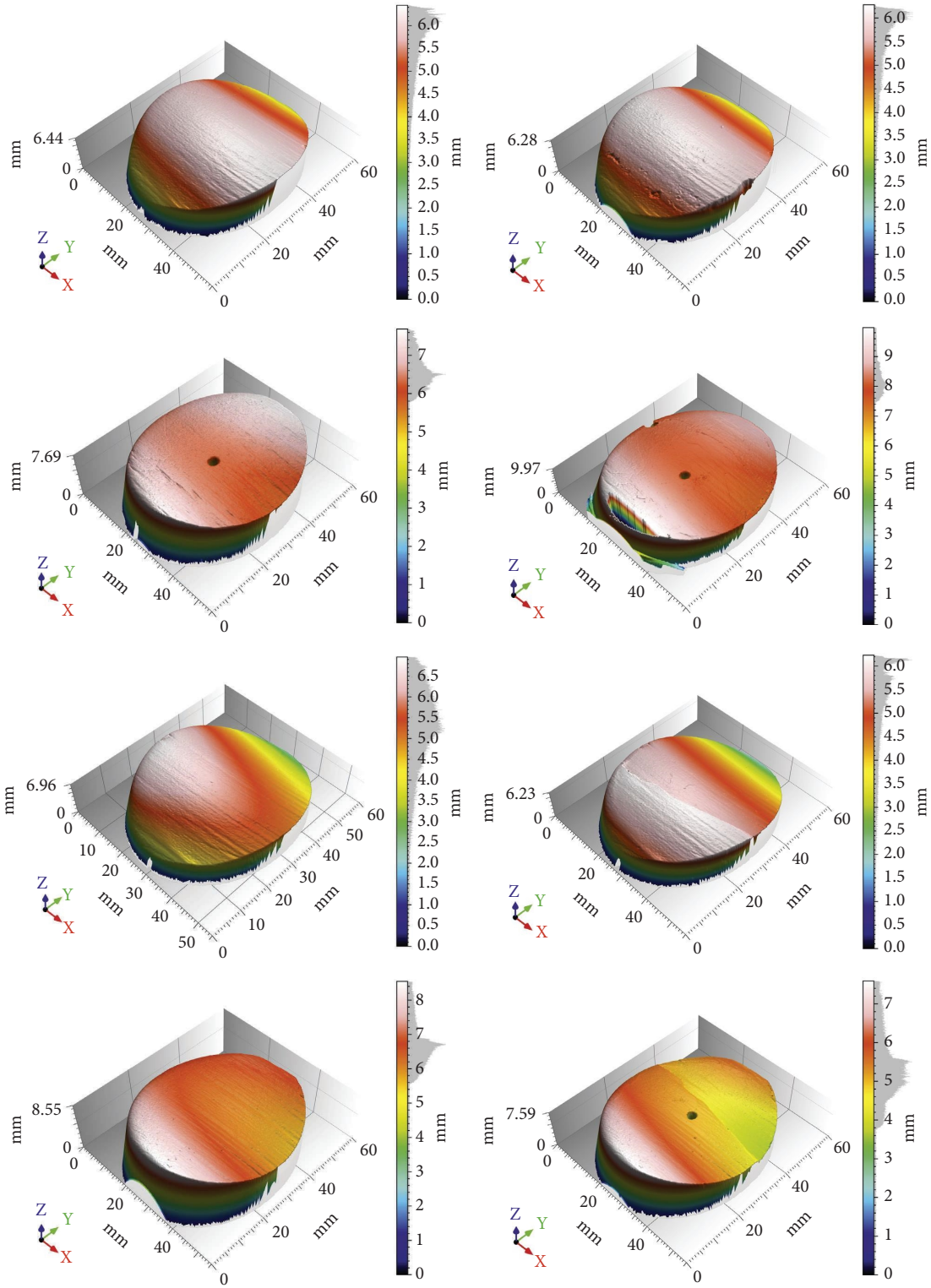

(c)

Figure 9: Continued.

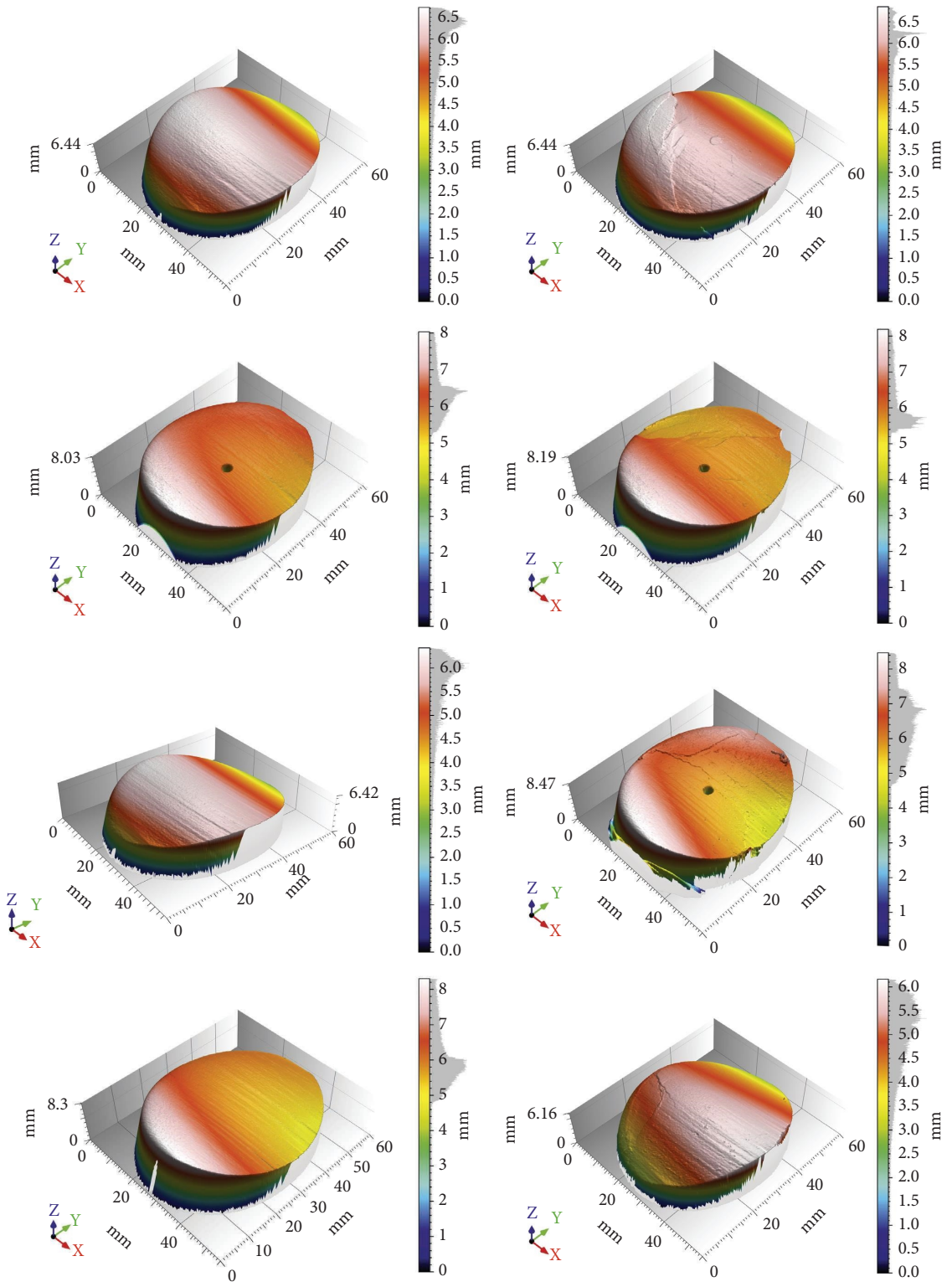

Figure 9: Three-dimensional view of joint plane scanning (the picture on the left is before the test, and the right is after the test).

Table 1: The change rate of joint rock morphology parameters (%).

Sample status	Pore water pressure (MPa) Morphology parameters	0	5	10	20	0	5	10	20
		The lower part of the sample (concave surface)				The upper part of the rock specimen (convex surface)			
Dry samples	S_q	31.88	−34.02	−0.62	−8.90	−14.80	−35.77	4.19	−13.88
	S_a	−6.22	−30.04	14.83	3.27	−13.00	−31.65	6.22	−11.65
	S_{mc}	−11.44	−29.05	18.38	−16.60	−16.05	−41.29	−7.45	4.02
	S_{al}	−4.78	−5.71	−0.03	−9.31	1.66	0.72	1.31	−0.87
Saturated samples	S_q	0.21	4.99	75.30	1.29	−24.06	−18.77	−7.87	−2.87
	S_a	3.78	2.59	67.57	9.20	−20.11	−14.16	−6.37	−0.61
	S_{mc}	3.48	−8.35	46.55	18.90	−29.41	−7.54	−5.26	2.79
	S_{al}	−0.24	−3.62	−9.52	4.35	0.40	−6.44	1.73	−2.86

plane morphology, affecting the destructional forms of the rock specimen.

5.1. Morphological Parameters of Jointed Rock Samples in Different States. Before and after the test, the upper and lower joint surfaces of the dry and saturated jointed rock samples were scanned in 3D morphology, as shown in Figure 9.

Under different water pressures, the dry sample nodal surface showed a transition from partial shear damage to overall shear damage, which was more obvious on the concave surface of the rock sample. When the pore water pressure was 0 MPa, there was only obvious shearing on the concave surface near the edge; when the pore water pressure was 5 MPa, the shearing range on the concave surface shifted toward the middle of the rock sample; when the pore water pressure was 10 MPa, the shearing range was already close to the middle line of the joint surface, indicating further expansion of the range; when the pore water pressure was 20 MPa, in addition to the shearing cracks extending toward the middle, there were secondary cracks produced on the concave surface This indicates that multiple damage occurred.

The cracks on the joint face of the saturated rock sample are more toward the middle, and the edges of the joint face in the lower half of the rock sample show obvious collapse cracks. At a pore water pressure of 0 MPa, there are obvious shear cracks on the convex surface, and the main crack in the middle of the concave surface derives several secondary cracks and a small part of chipping at the edge; at a pore water pressure of 5 MPa, in addition to a linear crack in the middle of the concave surface, small pieces of chipping appear at the junction between the crack and the edge of the joint surface; at a pore water pressure of 10 MPa, several small craters appear on the convex surface, indicating that the when the pore water pressure is 20 MPa, there are obvious shear cracks on the convex surface, and at the same time, there are cylindrical bumps in the middle due to the water pressure applied to the round hole of the concave surface, which indicates that the pore water pressure has a significant softening effect on the rock sample.

5.2. Analysis of morphological parameters. According to Table 1, it can be seen that the dry sample parameter S_q values are mainly decreasing under different water pressures, indicating that the dispersion of the height difference values at each point on the surface of the joint surface under the action of extrusion and friction decreases after the test. The saturated sample parameter S_q values were mainly decreasing in the upper part of the rock sample and increasing in the lower part of the rock sample, indicating that the test reduced the roughness of the convex surface and increased the roughness of the concave surface.

The dry sample parameter S_a value decreases when the pore water pressure is 0 MPa and 5 MPa, indicating that the average height of each point on the joint surface decreases, reflecting the reduction of the roughness of the joint surface by friction; it mainly shows an increase when the pore water pressure is 10 MPa and 20 MPa, mainly due to the misalignment of the sheared part. The saturation sample parameter S_a value also mainly decreases in the upper part of the rock sample and mainly increases in the lower part of the rock sample, indicating that the average height of the points on the convex surface decreases and the average height of the points on the concave surface increases. It reflects the decreasing effect of water pressure on the roughness of the rock sample.

From Table 1, it can be seen that the parameter S_q and S_a values of the upper half of the dry sample rock sample (convex surface) under the pore water pressure of 10 MPa have different trends from those under other pore water pressures. By observing the stress-strain curve of the dry sample at 10 MPa, it is found that the strain value increases the most from the stage of reaching the peak strength to the occurrence of damage, and at the same time, due to the local contact between the upper and lower parts of the through-variable dip joint surface, the rock sample joint surface produces the most relative sliding, which eventually leads to the increase of the roughness of the joint surface, and the parameter S*q* and S*a* values show a small increase.

The parameter S_{mc} value of the dry sample is mainly decreasing, reflecting the decrease of the curvature of the joint surface, which shows more wear in the middle for the convex surface, and indirectly reflects the shearing of the peak in the lower part of the rock sample for the concave surface. The saturated sample parameter S_{mc} values are also mainly decreasing in the upper half of the sample and increasing in the lower half of the sample, reflecting more wear in the middle than in the ends of the joint surface. This

indicates that the stress is more concentrated in the middle of the sample.

The S_{al} value of the dry sample decreases in the lower part of the sample and increases in the upper part, which indicates that the test process wears the lower part of the sample more obviously. The saturated sample parameter S_{al} value did not show a monotonic trend under different water pressure, which is due to the interaction of surface wear and shear part misalignment.

Different rock samples have different original roughness, so it is meaningful to compare the morphological scanning parameters of the same joint surface. The analysis of the rate of change of morphological parameters before and after the rock sample test shows that under different water pressure, the dry sample joint surface roughness decreases, the middle of the convex surface wears more, and the concave surface wears more obviously; the saturated sample convex surface roughness decreases, the concave surface roughness increases, and the middle of the joint surface wear is higher than the ends. There is no monotonic trend, the force in the middle of the joint surface of the rock sample is concentrated, and the joint surface appears partly misshapen.

6. Conclusion

This work mainly carries out the experimental research on the mechanical properties of variable dip angle jointed tuff rock samples, using the comparative analysis of mechanical properties of different types of rock samples and the analysis of surface morphological parameters of joints, etc. By establishing the dissolved pore model of tuff rock samples, the dry rock samples of variable dip angle jointed tuff were analyzed for factors such as variable pore water pressure, and the main conclusions obtained are as follows:

(1) The pore water pressure reaches the threshold value of 10 MPa before it produces a large deterioration of the strength of the dry nodular rock samples and has a significant effect on the rock properties. For saturated nodular rock samples, the effect of pore water pressure on strength is nonlinear, and the strength of rock samples only changes significantly when the pore water pressure changes by an order of magnitude. The main effect of pore water pressure is the deterioration of the rock sample and the change of frictional properties of the joint surface. Due to the smaller friction coefficient of the joint surface, the saturated rock samples are more prone to slip of the joint surface than the dry rock samples.

(2) In the case of applying lower pore water pressure, the elastic deformation is dominant in the deformation of dry jointed rock samples before reaching the peak strength. For saturated jointed rock samples, the application of pore water pressure can significantly increase the axial deformation of rock samples but weaken the elastic deformation and enhance the plastic deformation capacity of rock samples, and the higher pore water pressure has a more obvious effect on the deterioration of specimens. When the pore water pressure is higher, the rock samples show the characteristics of slip shear damage, and when the pore water pressure is lower, the rock samples are mainly in integral shear damage.

(3) Under different pore water pressure, the elastic modulus of saturated jointed rock samples fluctuates more, the elastic modulus of dry rock samples fluctuates less, and saturated rock samples are more sensitive to the change of pore water pressure. The dry nodular rock sample has a stronger deformation ability than the saturated nodular rock sample.

(4) Under different water pressure, the roughness of the dry sample nodular surface decreases, the middle of the convex surface is more worn, and the concave surface is worn more obviously; the roughness of the convex surface of the saturated sample decreases, the roughness of the concave surface increases, the middle of the nodular surface wear is higher than the two ends; there is no monotonic change trend, the force in the middle of the nodular surface of the rock sample is concentrated, and the nodular surface is partially misshapen.

Data Availability

The data (triaxial compression test) used to support the findings of this study are included within the supplementary information files.

Conflicts of Interest

The authors declare that they have no conflicts of interest.

Acknowledgments

This research was supported by the Joint Fund of the National Nature Science Foundation of China (U2034203), the Open Fund of the Key Laboratory of Geological Hazards on Three Gorges Reservoir Area (China Three Gorges University), Ministry of Education (2020KDZ12), the National Nature Science Foundation of China (52009067), the China National Natural Science Foundation Joint Funded Project (U1965109), and the Hubei Provincial Natural Science Foundation Innovation Group Project (2020CFA049).

Supplementary Materials

The following contents have been modified this time: the four formulas have been re-edited by Microsoft Word's formula editor. To represent Figure 9 more systematically, the numbers 3 and 4 have been moved to the original positions of the numbers 1 and 2. (*Supplementary Materials*)

References

[1] G. Duan, L. Wang, H. Deng, J. Zhang, Z. Luo, and Q. Jiang, "Mechanical response of listric faults in the three Gorges reservoir area based on three-dimensional morphological characteristics," *Frontiers in Physics*, vol. 9, Article ID 766920, 2021.

[2] G. Duan, Y. Wang, J. Chen, and J. Zhang, "Analysis of reservoir seismic law based on three-dimensional morphological characteristics of joint surface related to listric fault," *Frontiers in Physics*, vol. 9, Article ID 811609, 2022.

[3] J. Deng and L. Zhou, "Features and activity of Gaoqiao Fault zone along the north-western margin of zigui basin in Hubei province," *Geology and Mineral Resources of South China*, vol. 03, pp. 18–23, 2003.

[4] J. Xia, L. Zhou, and S. Liu, "Study on the characteristics and activity of main faults in Zigui Basin and its periphery in western Hubei province," *Hydrogeology & Engineering Geology*, vol. 01, pp. 10–14, 1996.

[5] L. Zhou and J. Z. J. Xia, "Characteristics of the Gaoqiao Fault zone and its influence of the three Gorges Project," *The people of the Yangtze river*, vol. 03, pp. 17–19, 1996.

[6] S. J. Gao, *Crustal Stress Field and Earthquakes in the Three Gorges Region of the Yangtze River Crustal Stress Field and Earthquakes in the Three Gorges Region of the Yangtze River*, 1992.

[7] L. H. Wang, "Experimental study on mechanical properties of jointed rock mass with different connectivity under triaxial loading and unloading," *Journal of rock mechanics and engineering*, vol. 34, no. 12, pp. 2500–2508, 2015.

[8] G. Duan, J. Li, J. Zhang, E. Assefa, and X. Sun, "Mechanical properties and failure modes of rock specimens with specific joint geometries in triaxial unloading compressive test," *Advances in Materials Science and Engineering*, pp. 1–14, Article ID 1340934, 2019.

[9] H. Rafiei Renani, C. D. Martin, and M. Cai, "An analytical model for strength of jointed rock masses," *Tunnelling and Underground Space Technology*, vol. 94, Article ID 103159, 2019.

[10] Y. Liu, F. Dai, L. Dong, N. W. Xu, and P. Feng, "Experimental investigation on the fatigue mechanical properties of intermittently jointed rock models under cyclic uniaxial compression with different loading parameters," *Rock Mechanics and Rock Engineering*, vol. 51, no. 1, pp. 47–68, 2018.

[11] X.-X. Yang and P. H. S. W. Kulatilake, "Laboratory investigation of mechanical behavior of granite samples containing discontinuous joints through direct shear tests," *Arabian Journal of Geosciences*, vol. 12, no. 3, p. 79, 2019.

[12] H. F. Deng, J. C. Fang, J. L. Li, Y. Xiao, and M. L. Zhou, "Influence mechanism of water state on mechanical properties of red bed soft rock," *Journal of coal*, vol. 42, no. 08, pp. 1994–2002, 2017.

[13] D. Hu, H. Zhou, Q. Hu, J. Shao, X. Feng, and H. Xiao, "A hydro-mechanical-chemical coupling model for geomaterial with both mechanical and chemical damages considered," *Acta Mechanica Solida Sinica*, vol. 25, no. 4, pp. 361–376, 2012.

[14] S. Rafieepour, H. Jalayeri, C. Ghotbi, and M. R. Pishvaie, "Simulation of wellbore stability with thermo-hydro-chemo-mechanical coupling in troublesome formations: an example from Ahwaz oil field, SW Iran," *Arabian Journal of Geosciences*, vol. 8, no. 1, pp. 379–396, 2015.

[15] R. Shen, T. Li, H. Li et al., "Study on the effect of water on electromagnetic radiation characteristics of fractured sandstone under load," *Environmental Earth Sciences*, vol. 80, no. 3, p. 87, 2021.

[16] X. Liu, L. Wu, Y. Zhang, Z. Liang, X. Yao, and P. Liang, "Frequency properties of acoustic emissions from the dry and saturated rock," *Environmental Earth Sciences*, vol. 78, no. 3, p. 67, 2019.

[17] A. Nicolas, J. Fortin, J. B. Regnet, A. Dimanov, and Y. Guéguen, "Brittle and semibrittle behaviours of a carbonate rock: influence of water and temperature," *Geophysical Journal International*, vol. 206, no. 1, pp. 438–456, 2016.

[18] Z. C. Tang, L. Li, X. C. Wang, and J. P. Zou, "Influence of cyclic freezing-thawing treatment on shear behaviors of granite fracture under dried and saturated conditions," *Cold Regions Science and Technology*, vol. 181, Article ID 103192, 2021.

[19] Y. Zhu, X. Liu, and E. Wang, "Influence of impoundment gravity and pore pressure on reactivation of faults," *Geomechanics and Geophysics for Geo-Energy and Geo-Resources*, vol. 6, no. 4, pp. 1–19, 2020.

[20] J. Li, J. Xu, L. Wang, H. Yang, and Z. Yang, "Water-rock coupling tests on mechanical properties of sandy slate rock mass," *Yantu Gongcheng Xuebao/Chinese Journal of Geotechnical Engineering*, vol. 35, no. 3, pp. 599–604, 2013.

[21] K. G. Li, "Experimental study on unloading damage and permeability characteristics of dolomite based on NMR technology," *Journal of rock mechanics and Engineering*, vol. 38, no. S2, pp. 3493–3502, 2019.

[22] X. Wang, W. Yuan, Y. Yan, and X. Zhang, "Scale effect of mechanical properties of jointed rock mass: a numerical study based on particle flow code," *Geomechanics and Engineering*, vol. 21, no. 3, pp. 259–268, 2020.

[23] J. Yu, X. Chen, Y.-y. Cai, and H. Li, "Triaxial test research on mechanical properties and permeability of sandstone with a single joint filled with gypsum," *KSCE Journal of Civil Engineering*, vol. 20, no. 6, pp. 2243–2252, 2016.